The development of a redox-sensitive curcumin conjugated chitosan oligosaccharide nanocarrier for the efficient delivery of docetaxel to glioma cells

Chunxi Liu[1#], Yuan Gao[2#], Lixia Zhao[1], Rui Wang[2], Fei Xie[1], Guangxi Zhai[2], Anchang Liu[1,3]^

[1]Department of Pharmacy, Qilu Hospital, Cheeloo College of Medicine, Shandong University, Jinan, China; [2]Department of Pharmaceutics, Key Laboratory of Chemical Biology, Ministry of Education, Shandong University, Jinan, China; [3]Department of Clinical Pharmacy, School of Pharmaceutical Sciences, Shandong University, Jinan, China

Contributions: (I) Conception and design: C Liu, Y Gao; (II) Administrative support: A Liu; (III) Provision of study materials or patients: Y Gao, R Wang; (IV) Collection and assembly of data: Y Gao, R Wang; (V) Data analysis and interpretation: Y Gao, C Liu, L Zhao, F Xie; (VI) Manuscript writing: All authors; (VII) Final approval of manuscript: All authors.

[#]These authors contributed equally to this work.

Correspondence to: Anchang Liu, PhD. Department of Pharmacy, Qilu Hospital, Cheeloo College of Medicine, Shandong University, 107 Wenhua West Rd., Jinan 250012, China. Email: acleu@126.com.

Background: A redox-sensitive nanoscale delivery system was developed, based on the hydrophilic chitosan oligosaccharide-ss-hydrophobic curcumin conjugate (CSO-ss-CUR) loaded with docetaxel (DTX), for the targeting and synergistic treatment of gliomas.

Methods: Redox-sensitive nanoparticles were loaded with DTX (DTX/CSO-ss-CUR) using the improved ultrasonic-dialysis approach. The morphology and particle size of the loaded nanoparticles were examined by transmission electron microscopy (TEM) and dynamic light scattering (DLS), respectively. The cytotoxicity and cellular uptake of the nanoparticles were assessed *in vitro* using the C6 glial cell line. The *in vivo* antitumor efficacy and *in vivo* biodistribution studies were evaluated using the C6 tumor-bearing Balb/c female mouse model.

Results: The DTX/CSO-ss-CUR nanoparticles were generally spherical in shape and exhibited desirable particle size (under 250 nm) with high drug loading efficiency (DL) (8.96%±0.56%) and encapsulation efficiency (EE) (35.23%±3.26%). *In vitro*, the drug was released from the nanoparticles in a redox-sensitive manner. The DTX/CSO-ss-CUR nanoparticles exhibited superior hemocompatibility in the hemolytic test and *in vitro* cytotoxicity and live/dead cell staining experiments revealed a higher cytotoxicity to glioma cells compared to the free drug. Furthermore, *in vitro* uptake experiments using C6 glioma cells demonstrated that the CSO-ss-CUR nanoparticles had good cell penetration ability. The *in vivo* antitumor efficacy and *in vivo* biodistribution studies suggested that the CSO-ss-CUR nanoparticles could effectively inhibit C6 tumor growth. More importantly, after intravenous injection, more CSO-ss-CUR nanoparticles were concentrated in the brain of the mice than free 1,1-dioctadecyl-3,3,3,3-tetramethylindotricarbocyanine iodide (DiR) group.

Conclusions: A unique drug delivery system formed by the self-assembly of CSO-ss-CUR was developed and shown to effectively cross the blood-brain barrier (BBB), enriching the abundance of the drug in the brain tissues. This may represent a potential therapeutic strategy for the treatment of gliomas.

Keywords: Chitosan oligosaccharide (CSO); curcumin (CUR); docetaxel (DTX); glioma

Submitted Nov 18, 2021. Accepted for publication Mar 01, 2022. This article was updated on October 10, 2024.
The original version is available at: http://dx.doi.org/10.21037/atm-22-288
doi: 10.21037/atm-22-288

^ ORCID: 0000-0003-2899-6260.

Introduction

Gliomas are the most common cancer of the central nervous system (1), accounting for approximately 80% of all malignant tumors arising in the brain (2). Malignant gliomas has a high incidence and aggressiveness, and present numerous challenges for treatment (3). Based on the World Health Organization (WHO) classification in 2016, there are four grades of gliomas (I to IV) and patients with grade-IV gliomas have an average survival time of only 15 months (4,5). Despite the multimodal therapeutic regimen of gliomas, including maximal surgical resection followed by concomitant radiotherapy or chemotherapy, treatment is usually insufficient to combat tumor progression (6). Due to the aggressive and infiltrating nature of gliomas, as well as the existence of blood-brain barrier (BBB) and the overexpression of P-glycoprotein (P-gp), malignant brain gliomas demonstrate limited response to antitumor therapy and result in high mortality rates (7,8). The presence of the BBB is the most crucial barrier restricting the entry of drugs in systemic brain-targeted delivery. Therefore, it is difficult to achieve the required concentration of chemotherapeutic drugs in the brain (9). In addition, the P-gp can pump the chemotherapeutic drugs outside the cell with the energy released from adenosine triphosphate (ATP) hydrolysis, thereby reducing the effective concentration of the drug in the cell and decreasing the sensitivity of tumor cells to chemotherapeutic drugs (10). Due to their hydrophobic and unstable nature, chemotherapeutic drugs used for glioma treatment have very low bioavailability, and thus, a large dose of the drug is often required which may lead to serious systemic toxic side reactions (2,11).

Various strategies have been explored to overcome the BBB for systemic drug delivery to cerebral tumors. Among them, novel nanoscale drug delivery systems that rely upon endogenous transport mechanisms have gained much interest. The ideal carrier for nanoparticles should be nontoxic and not stimulate any immune response, be biodegradable and biocompatible, have long plasma circulation times, can be adequately loaded with the drug, can protect the integrity of the drug, and have controlled release and targeting mechanisms (12). Natural polysaccharides which are direct or branched biopolymer polysaccharides composed of single or disaccharide repeat units have been widely used in the pharmaceutical as well as biomedical fields. These have the advantages of low toxicity, biodegradability, biocompatibility, and bioadhesion. In addition, many functional groups, including carboxyl, hydroxyl, and ammonia groups, are often found on the polysaccharide molecular backbone, allowing for easy modifications (13,14).

Chitosan oligosaccharide (CSO) is an oligomer of β-(1→4)-linked d-glucosamine, which is a degradation product of chitosan obtained by enzyme treatment with a polymerization degree of 2–10 (15). CSOs have recently been reported to possess various biological activities, including hypoglycemic, hypolipidemic, antioxidant, immune regulation, anti-inflammatory, antitumor, antibacterial, tissue engineering activities, and neuroprotective properties (16), and therefore may have extensive application prospects (17). CSO retains the advantages of chitosan, including being non-toxic and biodegradable. In addition, by reducing the molecular weight (MW), the water-solubility and bioactivity of CSO relative to chitosan can be improved, resulting in greater absorption and utilization by organisms. In addition, CSO is the only natural oligosaccharides with positive charges, it can easily bind to other molecules via hydrogen bonds and electrostatic interactions, which is responsible for many of their observed biological activities (18). Therefore, CSO-based nanoscale delivery systems have gained increasing attention in recent years (19). The molecular structure of CSO include functional groups such as ammonia, carboxyl groups, and hydroxyl groups that can be modified by small hydrophobic molecules to form amphiphilic polymers that can further self-assemble into polymer nanoparticles in water (20). More importantly, it has been reported that CSO and CSO-modified nanophotors can effectively cross the BBB (21).

Curcumin (CUR) is one of the main chemical constituents of turmeric (22). In recent years, the anti-cancer properties of CUR have been widely studied it have confirmed that CUR can inhibit the growth, invasion and metastasis of tumor cells and promoting tumor cell apoptosis via multiple signaling pathways. In addition, it has been reported CUR also can enhance the immune system (23). Thus, CUR is a promising drug for cancer therapy. Multiple studies have shown that CUR has low-toxicity and is an effective chemosensitizer in combination with multiple traditional cancer therapies, thereby increasing the therapeutic efficacy of the chemotherapeutic agent (24,25). CUR can also regulate P-gp activity through multiple pathways, such as inhibition of the PI3K/Akt/NF-B signaling pathway to sensitize chemotherapeutic agents (26-29). Therefore, the combination of CUR with classic anticancer drugs can reduce the efflux of the drug

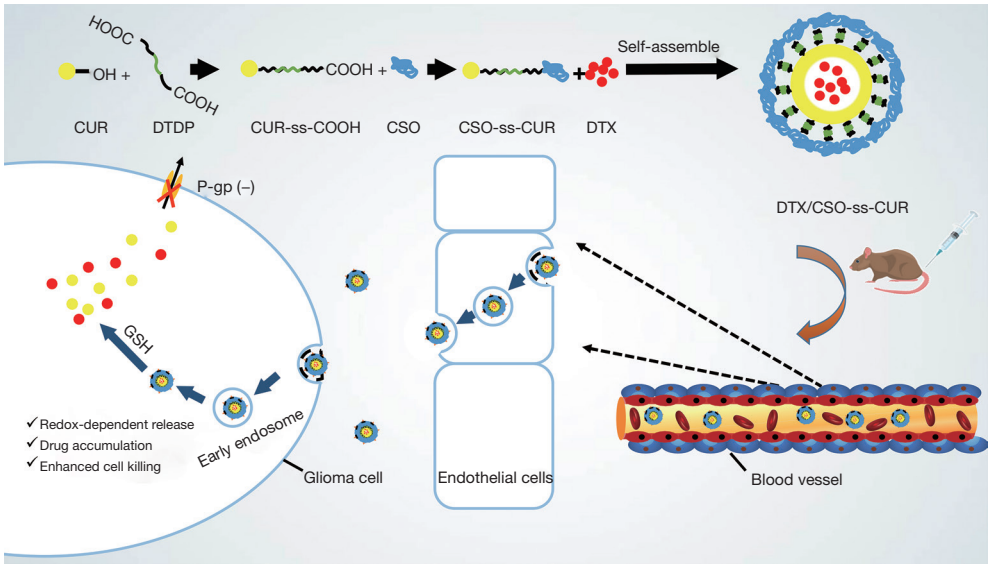

Figure 1 The rational design of the multifunctional, nanoscale delivery system (DTX/CSO-ss-CUR) for enhancing antitumor effects in glioma cells. CUR, curcumin; DTDP, 3,3'-dithiodipropionic acid; CSO, chitosan oligosaccharide; DTX, docetaxel; P-gp, P-glycoprotein; GSH, glutathione.

and increase drug sensitivity, and this is expected to become a novel, safe, and effective therapeutic strategy. Previous *in vitro* study has shown that CUR can improve the toxicity of paclitaxel in glial C6 cells and overcome the limitations of paclitaxel (30). Docetaxel (DTX) has certain therapeutic effect on a variety of cancers (31,32), including gliomas (33). However, due to the lack of tumor targeting, systemic administration of a simple DTX drug solution can cause significant damage to normal healthy tissues.

In the present study, a multifunctional, nanoscale delivery system, using CSO as a hydrophilic skeleton material, was designed for the treatment of glioma (*Figure 1*). The CSO and the hydrophobic small molecule drug CUR were coupled by disulfide bonds to form the amphiphilic polymer carrier material. The model drug DTX was packaged by self-assembly of the polymer material in water. The hydrophobic small molecule drug CUR not only acts as a part of the carrier material to form a hydrophobic cavity for the lipophilic chemotherapy drug DTX load, but also has antitumor and P-gp inhibitory effects which can enhance the chemotherapeutic sensitivity of DTX. Hydrophilic CSO prolongs the circulation times and increases the ability of the drugs to cross the BBB. The introduction of disulfide bonds as a redox-sensitive junction arm enables polymer nanoparticles to break in a highly reduced states within the tumor cells, enabling the efficient release of the chemotherapeutic agents at the tumor site. We present the following article in accordance with the ARRIVE reporting checklist (available at https://atm.amegroups.com/article/view/10.21037/atm-22-288/rc).

Methods

Materials

CUR was purchased from Alfa Aesar China (Tianjin) Co., Ltd. (China); CSO (MW =5,000 kDa) was purchased from Nantong Feiyu Biotechnology Co., Ltd. (China); and 3,3'-dithiodipropionic acid (DTDP) was purchased from Bide Pharmatech Ltd. (Shanghai, China). DTX was obtained from Baoji Guokang Biotechnology Co., Ltd. (China). The Cell Counting Kit-8 (CCK-8) and the Calcein-AM/PI Live/Dead staining kit were obtained from ApexBio Technology (USA). 6-diamidino-2-phenylindole (DAPI) was purchased from Genview (FL, USA) and 1,1-dioctadecyl-3,3,3,3-tetramethylindotricarbocyanine iodide (DiR) was procured from Yuheng Biochemicals Co., Ltd. (Suzhou, China). Dulbecco's modified Eagle's medium (DMEM) was obtained from Gibco BRL (Gaithersberg, MD, USA), while penicillin and streptomycin (1%), trypsin-EDTA (0.25%), phosphate and phosphate-buffered saline (PBS) were obtained from Solarbio Biotechnology Co., Ltd. (Shanghai, China). Plastic cell culture dishes, plates,

and flasks were obtained from Corning Inc. (Lowell, MA, USA). Paraformaldehyde (4%) was obtained from Biosharp Life Science (Hefei, China) and hematoxylin-eosin (H&E) stain was purchased from Beyotim Biotechnology (Shanghai, China). Double-distilled water was purified using the Millipore Simplicity System (Millipore, Bedford, MA, USA). All chemicals were of analytical or chromatographic reagent quality and purchased from commercial sources.

Cell lines and animals

The C6 rat brain glioma cell line was obtained from the Institute of Biochemical and Biotechnological Drugs of Shandong University. The C6 cells were cultured in DMEM containing 15% horse serum, 2.5% fetal bovine serum (FBS), and 1%/1% penicillin/streptomycin. All cells were maintained in a humidified incubator in an atmosphere of 5% CO_2 and 95% air.

Female Balb/c mice (aged 6–7 weeks and weighing 18–22 g) were supplied by Beijing Vital River Laboratory Animal Technology Co., Ltd. In our study, we have not fixed the gender either but chosen the more easily obtained ones under the experimental conditions at that time.

A protocol was prepared before the study without registration. All experiments were approved by the Research Ethics Committee of Qilu Hospital of Shandong University [No. KYLL-2021(ZM)-011], and were performed according to the Regulations of the People's Republic of China on the Management of Laboratory Animals (2017) for the care and use of animals. Authors were aware of group allocation at the different stages of the experiment.

Synthesis and characterization of polymers

Synthesis of dithiodipropionic anhydride (DTDPA)

A total of 0.5 g DTDP was refluxed in 3 mL acetyl chloride at 65 ℃ for 2 hours. After distilling most of the acetyl chloride under vacuum, the solution was precipitated into excess icy ethyl ether to remove the remaining acetyl chloride. After filtration to remove ethyl ether, the light yellow product was vacuum dried overnight to obtain the final DTDPA. The melting point test and ^{1}H nuclear magnetic resonance (NMR) were performed to estimate the successful synthesis of DTDPA.

Synthesis of CUR-ss-COOH

The single-ended carboxylated CUR containing the disulfide bond (-ss-) was synthesized by a modification of published protocols (34). The reaction was carried out under air free conditions. CUR (0.44 mmol) and 4-dimethylaminopyridine (DMAP) (0.16 mmol) were dissolved into 5 mL dry tetrahydrofuran (THF), followed by adding of 200 mL triethylamine. After stirring in the dark for 15 minutes, DTDPA (0.5 mmol) was dissolved into 1.5 mL THF and added into the reaction mixture drop by drop. The mixture was reacted for 24 hours at 70 ℃ in the dark under nitrogen protection. Finally, a dark red oil was obtained after removal of the organic solvents by rotary evaporation. The oil was collected using 10 mL ethyl acetate and washed with 5 mL HCl (pH 4). The organic layer was collected and the aqueous layer was washed with 10 mL ethyl acetate for three times. After removing the solvent using a rotatory evaporator, the final crude product was dissolved in 10 mL dichloromethane and loaded onto a silica gel column. The resulting compound of CUR-ss-COOH was isolated and purified by gradient elution with dichloromethane:methanol (CH_2Cl_2:CH_3OH =500:1–150:1) as a dark red solid.

Using glutaric anhydride (GA) as the linker instead of DTDPA, the single-ended carboxylated CUR not containing the disulfide bond (CSO-cc-COOH) was synthesized in the same way as that mentioned above. The chemical structures of CUR-ss-COOH and CUR-cc-COOH were confirmed by MS and ^{1}H NMR.

Synthesis of CSO-ss-CUR and CSO-cc-CUR

The single-ended carboxylated CUR was grafted to the backbone of the CSO through an amidation reaction to obtain a redox-sensitive amphiphilic CSO-ss-CUR polymer. In brief, CUR-ss-COOH (50 mg) was dissolved in 5 mL anhydrous dimethyl sulfoxide (DMSO), EDC was then added in and the reaction was stirred for 1 hour. Subsequently, NHS was added to activate the action for 3 hours to obtain an active ester solution. CSO was dissolved in 5 mL deionized water and the activated ester solution was slowly added into the CSO solution under rapid stirring and reacted for 24 hours at room temperature. Subsequently, the reactants were transferred into a dialysis bag [MW cut-off (MWCO) =2.0 kDa] for dialysis. Dialysis was initially performed against DMSO for 24 hours to remove free small molecules, followed by dialysis against deionized water for 72 hours to remove the organic solvents. Finally, further lyophilization was conducted to obtain CSO-ss-CUR. The non-redox-sensitive amphiphilic CSO-cc-CUR polymer was synthesized using the same

method as mentioned above using CSO-cc-COOH instead of CUR-ss-COOH. The chemical structures of CSO-ss-CUR and CSO-cc-CUR were confirmed by ^{1}H NMR and FT-IR.

The degree of substitution (DS) of CSO-ss-CUR or CSO-cc-CUR conjugate was defined as the number of CUR molecules per CSO molecule. The DS was determined by UV spectrometry using a standard curve generated with known concentrations of CUR in DMSO solution (35). Briefly, CUR was dissolved in the DMSO, several CUR solutions at concentrations of 2.0, 4.0, 6.0, 8.0, and 10.0 μg/mL were prepared for the calibration curve. CSO-ss-CUR and CSO-cc-CUR conjugate were dissolved in 1 mL DMSO, and the content of CUR in the conjugate was determined by UV spectrometry at 437 nm. The DS was calculated by Eq. [1]:

$$\mathrm{DS}\left(\mathrm{mol}\%\right)=\frac{\mathrm{M_{CSO}}\times\mathrm{m_{CUR}}}{\left(\mathrm{m_{polymer}}-\mathrm{m_{CUR}}\right)\times\mathrm{M_{CUR}}}\times 100\% \quad [1]$$

where m_{CUR} is the weight of CUR (mg); $m_{polymer}$ is the weight of CSO-ss-CUR or CSO-cc-CUR conjugate (mg); M_{CUR} is the MW of CUR; and M_{CSO} is the MW of the CSO unit.

Determination of the critical aggregation concentration (CAC)

The CAC of CSO-ss-CUR and CSO-cc-CUR were evaluated by fluorescence spectroscopy using pyrene as the hydrophobic fluorescence probe (36). Ten μL pyrene solution in acetone (0.015 mg/mL) was added to a series of colorimetric cylinders and the acetone was evaporated using nitrogen flow. Then, 5 mL of CSO-ss-CUR and CSO-cc-CUR conjugate solutions with concentration gradients of 1.5625, 3.125, 6.25, 12.5, 25, 50, 100, and 200 μg/mL were added to the colorimetric cylinders. All samples were stirred for 5 minutes using a laboratory vortex shaker and sonicated in an ultrasonic bath for 40 minutes to ensure proper mixing and dissolution of the compounds. The samples were then incubated overnight in the dark at room temperature. The fluorescence spectra of pyrene was obtained by a spectrophotometer (F-7000, Hitachi, Japan), and the slit-widths of excitation and emission were 10 and 2.5 nm, respectively. The emission spectra of pyrene was obtained at 300–450 nm with an excitation wavelength of 334 nm. The CAC of CSO-ss-CUR and CSO-cc-CUR conjugate solutions were calculated by extrapolating the cross point of the intensity ratio I_{373}/I_{384}.

Preparation of the DTX-loaded polymer nanoparticles

The DTX-loaded redox-sensitive (DTX/CSO-ss-CUR) nanoparticles were prepared by an improved ultrasonic-dialysis method (37). Briefly, 10 mg CSO-ss-CUR was dissolved in 5 mL deionized water and stirred for 30 minutes in the dark at room temperature. DTX, dissolved in 1 mL DMSO, was slowly added drop by drop into the CSO-ss-CUR solution. The mixture was then stirred for a further 4 hours in the dark followed by ultrasonication for 30 minutes (100 w, 2 s/2 s) in an ice bath. The mixture was then placed into a dialysis bag (MWCO =2.0 kDa) and dialyzed using deionized water for 24 hours to remove the DMSO and the unentrapped DTX. The solution was lyophilized to obtain the DTX loaded polymer nanoparticles after centrifugation (3,500 rpm for 10 minutes). The DTX-loaded non-redox-sensitive (DTX/CSO-cc-CUR) nanoparticles were prepared using the methods described above.

The size distribution, particle dispersion index (PDI) and zeta potential of the DTX-loaded polymer nanoparticles were measured by dynamic light scattering (DLS). The particle morphology was observed by transmission electron microscopy (TEM; JEM-2010, Japan).

The redox-sensitivity of the blank CSO-ss-CUR nanoparticles was investigated under reductive conditions. After incubation with 10 mM dithiothreitol (DTT) for 12 and 24 hours in a constant temperature shaker with a rotating speed of 100 rpm at 37 ℃, the size and PDI were further determined using DLS to serve as redox-sensitivity indicators.

Drug encapsulation efficiency (EE) and loading efficiency (DL)

DTX/CSO-ss-CUR or DTX/CSO-cc-CUR nanoparticles (300 μL) were dispersed in an equal volume of DMSO and ultrasonicated for 2 minutes on an ice bath to destroy the structure of the nanoparticles. After cooling to room temperature, 1 mL of methanol was added. The content of the encapsulated DTX was determined by HPLC at 230 nm. The drug EE and DL were calculated using Eqs. [2,3], respectively:

$$\mathrm{EE}\left(\%\right)=\frac{\mathrm{W_{loaded\ DTX}}}{\mathrm{W_{added\ DTX}}}\times 100\% \quad [2]$$

$$\mathrm{DL}\left(\%\right)=\frac{\mathrm{W_{loaded\ DTX}}}{\mathrm{W_{polymer}}+\mathrm{W_{loaded\ DTX}}}\times 100\% \quad [3]$$

where $W_{added\ DTX}$ is the total amount of DTX added; $W_{loaded\ DTX}$ is the content of encapsulated DTX; and $W_{polymer}$ is the weight of polymer nanoparticles.

In vitro release of the DTX-loaded nanoparticles

The *in vitro* release experiment was carried out in PBS buffer (pH 7.4) containing 0.5% Tween 80. Briefly, freshly prepared DTX/CSO-ss-CUR and DTX/CSO-cc-CUR nanoparticles (containing about 30 μg of DTX) were put into a dialysis bag (MWCO =2.0 kDa) and immersed in 25 mL release medium containing different concentrations of DTT and gently shaken in a constant temperature shaker with a rotating speed of 100 rpm at 37 ℃. At the predetermined time points, 0.5 mL of the sample was removed and replaced with an equal volume of fresh release medium. Samples were then filtered with a 0.22 μm microporous membrane and the released amount of DTX was determined by HPLC method as described above.

Evaluation of the hemolysis of the nanoparticles

Two percent erythrocytes suspension extracted from fresh rabbit blood was used to evaluate the hemolysis of the nanoparticles (38). A series concentrations of DTX/CSO-ss-CUR nanoparticles were added into each tube containing 0.5 mL erythrocytes suspension, and the total volume was kept at 1 mL. Meanwhile, distilled water or normal saline (NS) solution was mixed with the erythrocyte suspensions to prepare a positive and negative group, respectively. After incubated for 1 hour at 37 ℃, the mixed suspensions were centrifuged at 3,000 rpm for 10 minutes to remove the intact erythrocytes. Then, the supernatant was collected following by analysis using UV/vis spectrophotometer at 541 nm. The degree of hemolysis was calculated using Eq. [4]:

$$\text{Hemolysis rate}(\%) = \frac{A_{sample} - A_{negtive}}{A_{positive} - A_{negtive}} \times 100\% \quad [4]$$

where A_{sample}, $A_{positive}$, and $A_{negative}$ are the absorbance of the sample, absorbance of a solution which has undergone 100% hemolysis, and absorbance of a solution with 0% hemolysis, respectively. A sample solution without erythrocytes was used as a blank control to compensate the turbidity of the conjugate samples.

In vitro cytotoxicity and live/dead cell staining

CCK-8 assays were performed to determine the cell viability of C6 cells. C6 cells were seeded in 96-well plates (8×10^3 cells/well) and cultured overnight. Free DTX, DTX/CSO-cc-CUR nanoparticles, and DTX/CSO-ss-CUR nanoparticles were diluted to a series different concentration of DTX by the culture medium. Positive control group (culture medium and cells, no formulations) and negative control group (culture medium alone, no cells or formulations) were set up. After incubation for 24 hours, 10 μL of CCK-8 was added and incubated for 1 hour, and the optical density (OD) values were determined using a microplate reader at 450 nm. The cell viability was calculated using Eq. [5] and the half maximal inhibitory concentration (IC_{50}) values were obtained using the cytotoxicity curves.

$$\text{Cell viability}(\%) = \frac{OD_{sample} - OD_{negative}}{OD_{positive} - OD_{negative}} \times 100\% \quad [5]$$

where $OD_{negative}$, $OD_{positive}$, and OD_{sample} are the OD values of the negative control, positive controls, and samples, respectively.

The live/dead cell staining assay was also performed to determine the cell cytotoxicity of C6 cells. C6 cells were seeded in 12-well plates (1×10^5 cells/well) and cultured overnight. Cells were treated with 1 mL free DTX (5 μg/mL), DTX/CSO-ss-CUR nanoparticles, or DTX/CSO-cc-CUR nanoparticles for 24 hours. The cells were then washed with PBS for three times and stained with calcein-AM and propidium iodide (PI) according to the manufacturer's instructions.

Intracellular uptake

Cellular uptake was assessed using the tracer agent C6 and visualized under a fluorescent inverted microscope (Olympus, Tokyo, Japan). C6 cells were seeded into 12-well culture plates and incubated overnight. The culture medium was then replaced with 1 mL of fresh medium containing C6-loaded CSO-ss-CUR nanoparticles or free C6 solution at the same concentration (2 μg/mL). After incubation for 2 and 4 hours, the cells were washed with PBS and fixed with 4% paraformaldehyde for 10 minutes. Cells were washed with PBS three times and incubated with 150 μL

DAPI at room temperature for 5 minutes. The cells were then washed and qualitatively observed using a fluorescent inverted microscope.

In vivo antitumor efficacy

To evaluated the antitumor efficacy, C6 tumor-bearing Balb/c female mouse model was established. Balb/c female mice were subcutaneously inoculated with C6 cells to establish the xenograft glioma model. When the tumor volume reached 100 mm^3, twenty mice were randomly divided into four groups (n=5). The mice were administered the following via tail vein injection every 3 days for four times: NS, free DTX (Taxotere®), DTX/CSO-ss-CUR nanoparticles, or DTX/CSO-cc-CUR nanoparticles (10 mg DTX equiv./kg). The dose of CSO-ss-CUR in xenograft glioma model was determined according to the previously published litterateurs (39-41). No mice died or needed to be terminated 24 h after NPs administration. The tumor volume and body weight were measured before each administration. On day 12 after the first administration, the mice of different groups were sacrificed and the tumors were excised, washed, photographed, and weighed. The tumor inhibition rate (Ti) was calculated by Eq. [6] for different groups:

$$\mathrm{Ti}(\%) = (\mathrm{Vs} - \mathrm{Vi})/\mathrm{Vs} \times 100\% \quad [6]$$

where Ti represents the tumor inhibition rate; Vs represents the mean tumor volume of the NS group; and Vi represents the mean tumor volume of different groups.

Immunohistochemistry evaluation

After the *in vivo* antitumor efficacy study, the mice were then euthanized, and major organs of mice including the brain, heart, liver, kidney, and spleen, as well as the tumors were excised, washed, fixed in 4% paraformaldehyde, and embedded in paraffin wax for histological analysis. The sections were stained with H&E. In addition, the tumor sections were stained with Ki67 to evaluate cell proliferation.

In vivo biodistribution of DTX-loaded nanoparticles

the biodistribution of the drugs was observed by real-time near-infrared fluoroscope (NIRF) imaging. A near-infrared fluorophore dye (DiR) was used to replace DTX in the formulation. DiR loaded nanoparticles (DiR/CSO-ss-CUR) were prepared as described previously to obtain a final DiR concentration of 50 μg/mL. The free DiR was dissolved in methanol (1 mg/mL) and diluted to 50 μg/mL. Balb/c female mice were injected intravenously with free DiR or DiR/CSO-ss-CUR (0.1 mL). After 1, 2, and 4 hours, the mice were anesthetized with 10% chloral hydrate (i.p.) and observed. Thereafter, the mice were sacrificed and the major organs (heart, brain, liver, spleen, and kidney) were excised for *in vitro* imaging. The real-time NIRF images were tested using a real-time NIRF detector (Caliper Life Sciences, USA) at appropriate wavelengths (excitation wavelength of 745 nm, emission wavelength of 835 nm).

Statistical analysis

The Student's *t*-test was used to analyze the statistical differences. And P value <0.05 was considered statistically significant. All data were showed as the mean ± standard deviation (SD).

Results

Preparation and characterization of the CSO-ss-CUR conjugate

CUR was conjugated with CSO-ss-COOH by an amide bond. The chemical structure of CSO-ss-CUR was verified by ^{1}H NMR and FT-IR spectroscopy. *Figure 2A* shows the ^{1}H NMR spectra of CUR, CSO, CSO-ss-CUR, and CSO-cc-CUR. The typical signals for CUR were observed, including the -CH_2- peaks (δ =6.49–6.51 ppm), -CH- peaks (δ =6.99–7.00 ppm), -CH- peaks (δ =7.55–7.60 ppm), -CH- peaks (δ =7.12–7.14 ppm), -CH- peaks (δ =7.10–7.11 ppm), -CH- peaks (δ =7.11–7.12 ppm), and the -CH_3 peaks (δ =3.98 ppm). The characteristic peaks of aromatic protons (a) were detected at δ 7.10–7.14 ppm of CUR. In *Figure 2A*, the characteristic peaks of the sugar ring were observed at δ 2.89–4.10 ppm of CSO. The characteristic peaks of aromatic protons from CUR (δ 6.78–7.54 ppm) and the sugar ring from CSO (δ 3.23–4.65 ppm) were simultaneously observed in the spectrum of CSO-ss-CUR and CSO-cc-CUR, indicating the successful modification of CUR. By calculating the number of CUR molecules per CSO molecule using UV spectrometry, the DS of CUR in CSO-ss-CUR and CSO-cc-CUR were found to be 15.09%±0.83% and 16.45%±1.29%, respectively.

FT-IR was used to demonstrate the synthesis of the conjugates (*Figure 2B*). The peak at 3,378.32 cm^{-1} can be

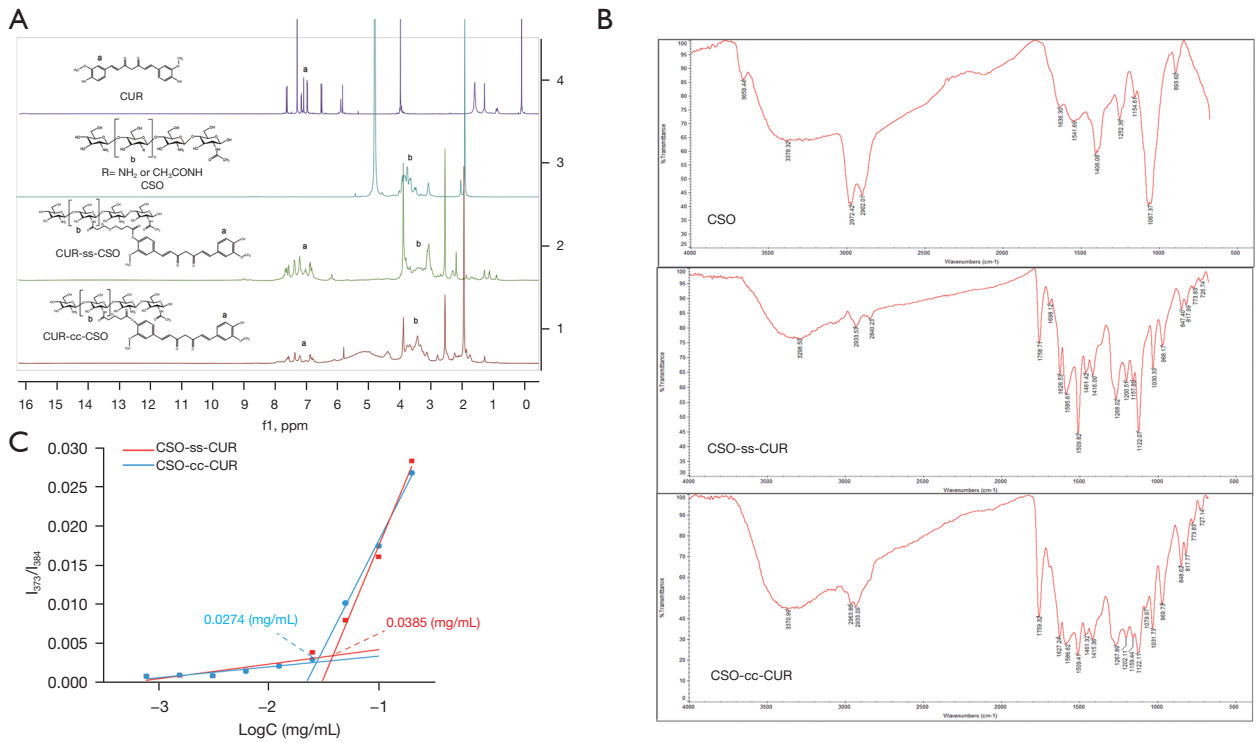

Figure 2 The structure confirmation and the CAC of CSO-ss-CUR and CSO-cc-CUR. (A) The ^{1}H NMR spectra of CUR, CSO, CSO-ss-CUR, and CSO-cc-CUR. (B) The FTIR spectra of CSO, CSO-ss-CUR, and CSO-cc-CUR. (C) The fluorescence intensity ratio (I_{373}/I_{384}) of pyrene at different concentrations of CSO-ss-CUR and CSO-cc-CUR. CUR, curcumin; CSO, chitosan oligosaccharide; CAC, critical aggregation concentration; NMR, nuclear magnetic resonance; FTIR, fourier transform infrared spectroscopy.

ascribed to the mixed stretching vibration peak of O-H and N-H, the peak at 1,636.30 cm^{-1} is the stretching vibration absorption peak of C=O, the strong absorption peak at 1,067.37 cm^{-1} is the stretching vibration of O-C in the primary and secondary alcohols, and the characteristic peaks at 893.60 cm^{-1} are the typical sugar ring peaks. Compared with the CSO spectrum, the new peaks at 1,758.71 cm^{-1} in the CSO-ss-CUR spectrum and at 1,759.32 cm^{-1} in the CSO-cc-CUR spectrum represent the stretching vibration absorption peak of the C=O of the amide bond, demonstrating that the free amine groups of CUR had been successfully conjugated to the CSO. Additionally, the peaks at 1,200.51 cm^{-1} in the CSO-ss-CUR spectrum and at 1,202.11 cm^{-1} in the CSO-cc-CUR spectrum are characteristic of the phenolic hydroxyl of CUR, further confirming the conjugation of CUR to the backbone of CSO.

The CAC of CSO-ss-CUR and CSO-cc-CUR

CAC was used to evaluated the self-assembly behavior of the CSO-ss-CUR and CSO-cc-CUR in aqueous solution and the dilution resistance capacity. *Figure 2C* shows the plots of I_{373}/I_{384} versus the logarithm concentration of CSO-ss-CUR and CSO-cc-CUR. As shown in the plots, at the beginning, the I_{373}/I_{384} ratio increased slowly with increasing concentrations. However, the ratio of I_{373}/I_{384} then increased abruptly when the concentration reached a certain value, and the turning point was the CAC. From the plots, the CAC values of CSO-ss-CUR and CSO-cc-CUR were calculated to be 0.0196 and 0.0173 mg/mL, respectively.

Preparation and characterization of the DTX-loaded nanoparticles

DTX-loaded CSO-ss-CUR nanoparticles with varied drug/carrier ratios (w/w) were synthesized using an improved ultrasonic-dialysis approach. The influence of the drug/carrier ratio (w/w) on the DL and EE values of the DTX-loaded CSO-ss-CUR nanoparticles is summarized in *Table 1*. Increasing DTX/CSO-ss-CUR ratio (w/w) was associated

with an increased trend for the DL. When the DTX/CSO-ss-CUR ratio (w/w) increased from 1:10 to 3:10, the DL increased from 2.13%±0.54% up to 8.96%±0.56%, indicating good drug loading capacity of this nanocarrier system. The upward trend of the DL could be attributed to the enhanced hydrophobic interaction between DTX and CSO-ss-CUR. However, the EE increased first and then decreased. When the DTX/CSO-ss-CUR ratio increased from 1:10 to 2:10, the EE increased from 33.63%±1.21% to 40.27%±4.00%. However, when the DTX/CSO-ss-CUR ratio increased from 2:10 to 3:10, the EE decreased to 35.23%±3.26%. The decrease of EE may be due to the excessive feeding of DTX exceeding the maximum drug loading capability of CSO-ss-CUR. Thus, to simultaneously obtain a higher DL and EE, a 3:10 ratio of DTX/CSO-ss-CUR (w/w) was used to prepare DTX-loaded CSO-ss-CUR nanoparticles for further studies.

The mean particle size, PDI, and zeta potential of various formulations are shown in *Table 2*. The particle size distribution of each formulation characterized by DLS is concentrated around 200 nm (*Figure 3A*) with a PDI of less than 0.3, suggesting that the prepared nanoparticles were uniform.

TEM was used to observe the nanoparticles (*Figure 3B*). Most blank and drug-loaded nanoparticles were generally spherical, separated, and homogeneously distributed, indicating stable formulations.

CSO-ss-CUR was incubated for 12 or 24 h with or without 10 mM DTT, and the particle size distribution was examined (*Figure 3C*). The results showed that for nanoparticles without DTT, there was only a slight change in particle size, from 180.7 to 185.1 nm, with a few increases of PDI, indicating good formulation stability. However, in the presence of 10 mM DTT, the particle size distribution changed from a single peak to multiple peaks, with particles less than 100 nm in size after a 24-hour incubation, indicating that the disulfide bonds in the CSO-ss-CUR nanoparticles had been destroyed under reductive conditions, and the formed nanopore structure was loose and expanded with partially degraded debris and particle aggregation.

Table 1 The influence of the drug/carrier ratio (w/w) on the DL and EE values of DTX-loaded CSO-ss-CUR nanoparticles (n=3)

Sample	DTX:CSO-ss-CUR (w/w)	DL (%)	EE (%)
DTX/CSO-ss-CUR	1:10	2.13±0.54	33.63±1.21
	2:10	4.86±0.74	40.27±4.00
	3:10	8.96±0.56	35.23±3.26

DL, drug loading efficiency; EE, encapsulation efficiency; DTX, docetaxel; CSO, chitosan oligosaccharide; CUR, curcumin.

In vitro release of DTX-loaded nanoparticles

The drug release behavior of the DTX-loaded nanoparticles was investigated in PBS (pH 7.4) with or without 10 mM DTT. As represented in *Figure 3D*, 42.86%±2.22% DTX was released during the 24-hour incubation without DTT. In comparison, for nanoparticles incubated with DTT, 71.13%±3.56% DTX was released after 24 hours. During 72 hours of incubation, only 60.75%±9.34% DTX were cumulatively released without DTT, while the cumulative release percentage of DTX with DTT was up to 87.94%±3.84%.

Biocompatibility study

To estimate blood stability, the hemolysis rate of CSO-ss-CUR nanoparticles was studied (*Figure 3E*). The hemolysis rate for different concentrations of nanoparticles (0.1 to 1 mg/mL) was consistently below 5% compared with the negative control group, indicating the superior hemocompatibility of the nanoparticles.

In vitro cytotoxicity and live/dead cell staining

The *in vitro* cytotoxicity of DTX/CSO-ss-CUR and DTX/CSO-cc-CUR nanoparticles was studied and compared to

Table 2 Characteristics of the different nanoparticles (n=3)

Samples	Size (nm)	PDI	Zeta potential (mV)
CSO-ss-CUR nanoparticles	189.5±4.78	0.073	3.33±2.01
DTX/CSO-ss-CUR nanoparticles	213.8±5.23	0.192	3.21±1.54
DTX/CSO-cc-CUR nanoparticles	232.1±4.67	0.223	3.35±0.26

CSO, chitosan oligosaccharide; CUR, curcumin; DTX, docetaxel; PDI, particle dispersion index.

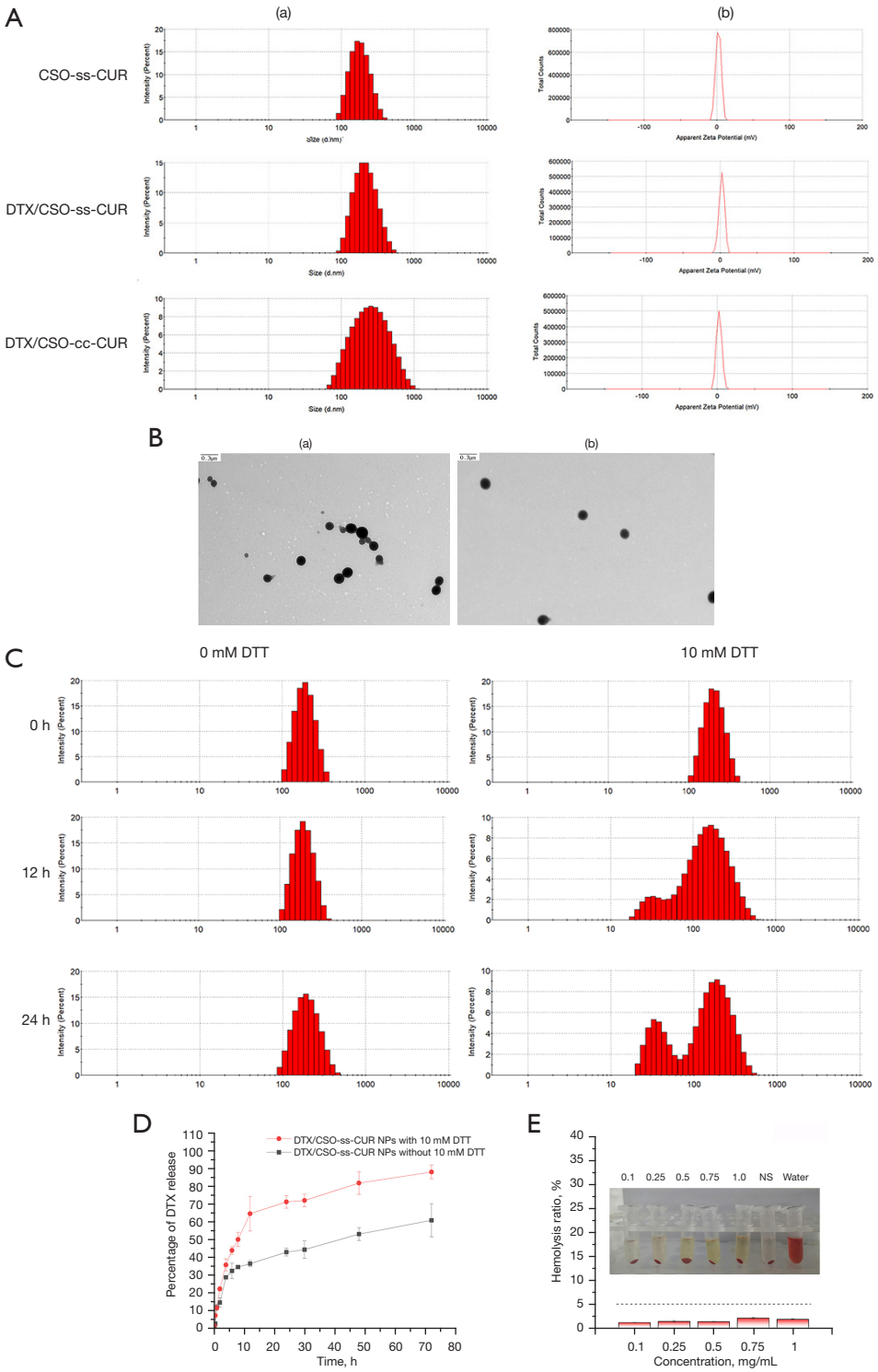

Figure 3 The physicochemical properties, drug release behavior and hemolysis characterization of nanoparticles. (A) Size distribution (a) and zeta potential (b) of the nanoparticles. (B) TEM image of blank (a) and DTX/CSO-ss-CUR nanoparticles (b). (C) The size distribution of CSO-ss-CUR nanoparticles incubated for 12 and 24 hours with or without 10 mM DTT. (D) *In vitro* DTX release profile of DTX-loaded nanoparticles in the presence and absence of 10 mM DTT. (E) Hemolytic analysis of CSO-ss-CUR nanoparticles. CSO, chitosan oligosaccharide; CUR, curcumin; DTX, docetaxel; DTT, dithiothreitol; NPs, nanoparticles; NS, normal saline; TEM, transmission electron microscopy.

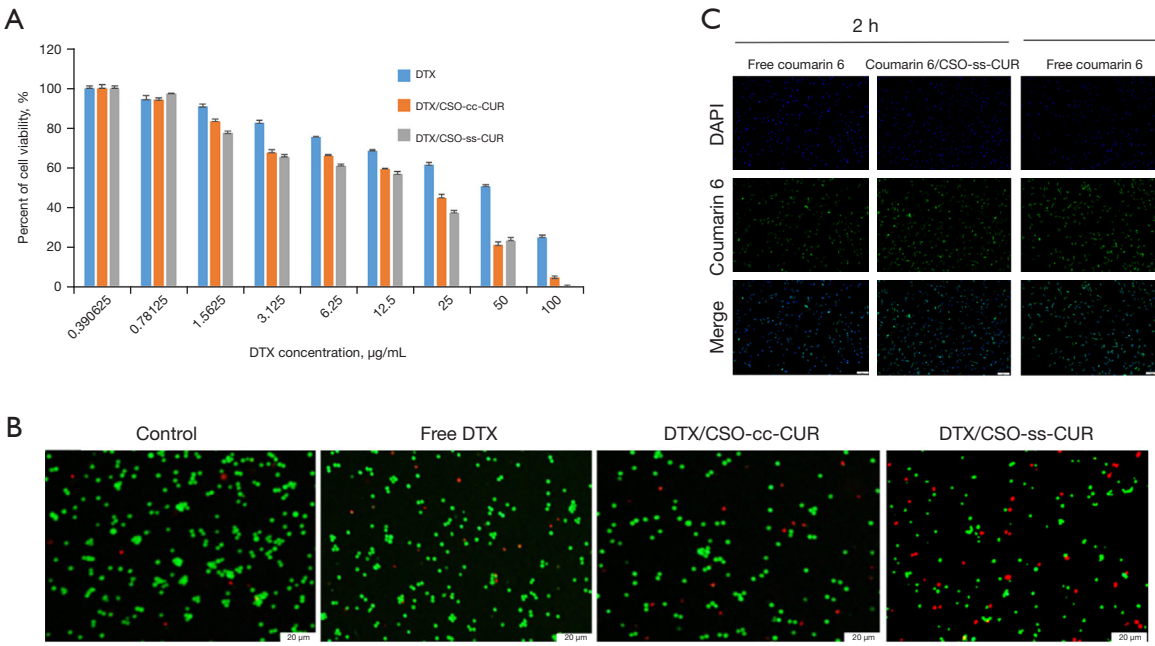

Figure 4 The *in vitro* cytotoxicity, live/dead cell staining and the intracellular uptake of nanoparticles. (A) Cell viability of C6 rat glioblastoma cells in response to treatment with DTX, DTX/CSO-cc-CUR, or DTX/CSO-ss-CUR nanoparticles for 24 hours (n=6). (B) Live/dead staining results of C6 cells after 24 hours treatment with free DTX, DTX/CSO-cc-CUR, and DTX/CSO-cc-CUR nanoparticles. (Scale bar: 20 μm). (C) Cell uptake of free coumarin 6 and coumarin 6-loaded CSO-ss-CUR nanoparticles after incubation for 2 and 4 hours. (Scale bar: 50 μm). DTX, docetaxel; CSO, chitosan oligosaccharide; CUR, curcumin.

Table 3 The IC_{50} values of free DTX, DTX/CSO-cc-CUR, and DTX/CSO-ss-CUR nanoparticles against C6 glioma cell over 24 hours

Samples	IC_{50} (μg/mL)	RRI*
Free DTX	25.29	–
DTX/CSO-cc-CUR nanoparticles	10.52	2.404
DTX/CSO-ss-CUR nanoparticles	8.694	2.909

*, RRI = IC_{50} (free DTX)/IC_{50} (nanoparticles). IC_{50}, half maximal inhibitory concentration; DTX, docetaxel; CSO, chitosan oligosaccharide; CUR, curcumin; RRI, resistance reversion index.

free DTX at the same equivalent drug concentration in C6 glioma cells. Both free DTX and nanoparticles reduced the viability of C6 glioma cells after 24 hours of exposure (*Figure 4A*). With increasing DTX concentrations, there was an increased inhibition of cancer cell proliferation. These observations suggested that free DTX and nanoparticles had concentration-dependent cytotoxic effects on C6 glioma cells. The IC_{50} values of free DTX, DTX/CSO-ss-CUR, and DTX/CSO-cc-CUR nanoparticles against C6 cells after 24 hours are listed in *Table 3*. Both DTX/CSO-cc-CUR nanoparticles and DTX/CSO-ss-CUR nanoparticles showed a lower IC_{50} value compared with free DTX, indicating higher cytotoxicity (*Table 3*).

The resistant ability of nanoparticles against C6 cells was confirmed by resistance reversion index (RRI). The RRIs of DTX/CSO-cc-CUR and DTX/CSO-ss-CUR nanoparticles were 2.404 and 2.909, respectively. To further elucidate the antitumor activity of DTX-loaded nanoparticles, a live/dead cell assay was conducted to evaluate the cytotoxic effect of nanoparticles on C6 glioma cells, with dead cells staining red and living cells staining green. Cell treated with DTX/CSO-ss-CUR and DTX/CSO-cc-CUR nanoparticles showed significantly higher red fluorescence compared to cells treated with free DTX (*Figure 4B*), indicating that the nanoparticles had greater cytotoxicity compared to free DTX. Indeed, combination therapy may have obvious advantages over single drug therapy.

Intracellular uptake

Since the fluorescence of CUR is very fragile and easily

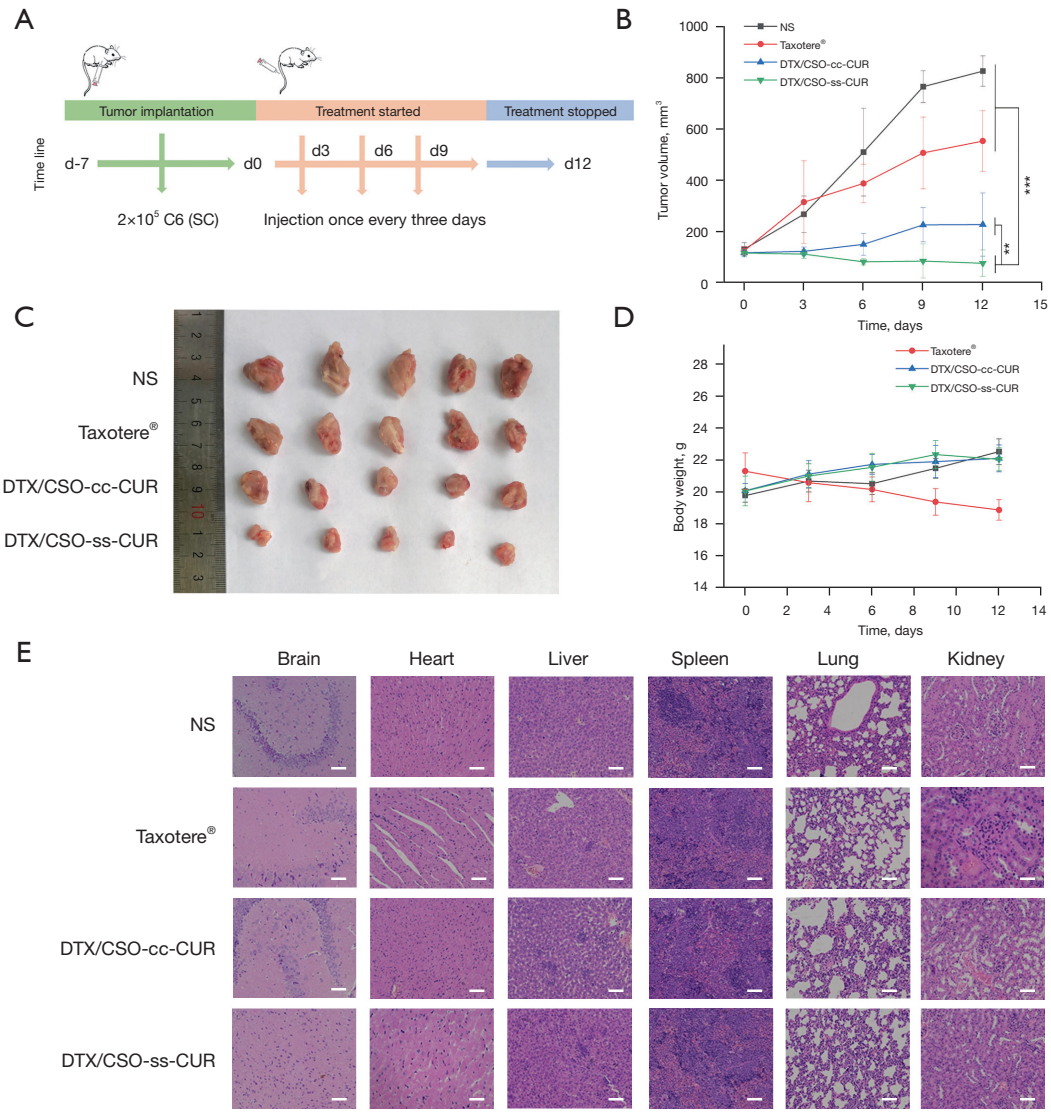

Figure 5 The *in vivo* antitumor efficacy and the immunohistochemistry results of nanoparticles. (A) Schematic representation of the *in vivo* study protocol. (B) Quantified tumor size of mice by volume measurements. Data are presented as the mean ± SD (n=5; **P<0.05, and ***P<0.001). (C) Digital photographs of tumor tissues following various treatments. (D) Body weight change curves (n=5). (E) Histological H&E staining of the major organs excised from tumor-bearing mice treated with NS, Taxotere®, DTX/CSO-cc-CUR nanoparticles, DTX/CSO-ss-CUR nanoparticles (scale bar: 200 μm). NS, normal saline; DTX, docetaxel; CSO, chitosan oligosaccharide; CUR, curcumin; SD, standard deviation; H&E, hematoxylin-eosin.

quenched, C6 was encapsulated into CSO-ss-CUR nanoparticles to evaluate the *in vitro* cellular uptake. After 2 hours, the green fluorescence intensity was comparable between cells incubated with free C6 and cells incubated with the C6-encapsulated nanoparticles (*Figure 4C*). After 4 hours, cells incubated with the C6-encapsulated/CSO-ss-CUR nanoparticles showed intense fluorescence compared to cells treated with free C6.

In vivo antitumor efficacy

The antitumor efficacy of the DTX/CSO-ss-CUR nanoparticles was investigated by assessing tumor growth in a mouse model (*Figure 5A*). Tumors in control animals grew rapidly, from 130.31±25.21 mm^3 on the initial day to 823.02±59.62 mm^3 on day 12. The tumors in the free DTX (Taxotere®) group grew from 123.98±15.76 to

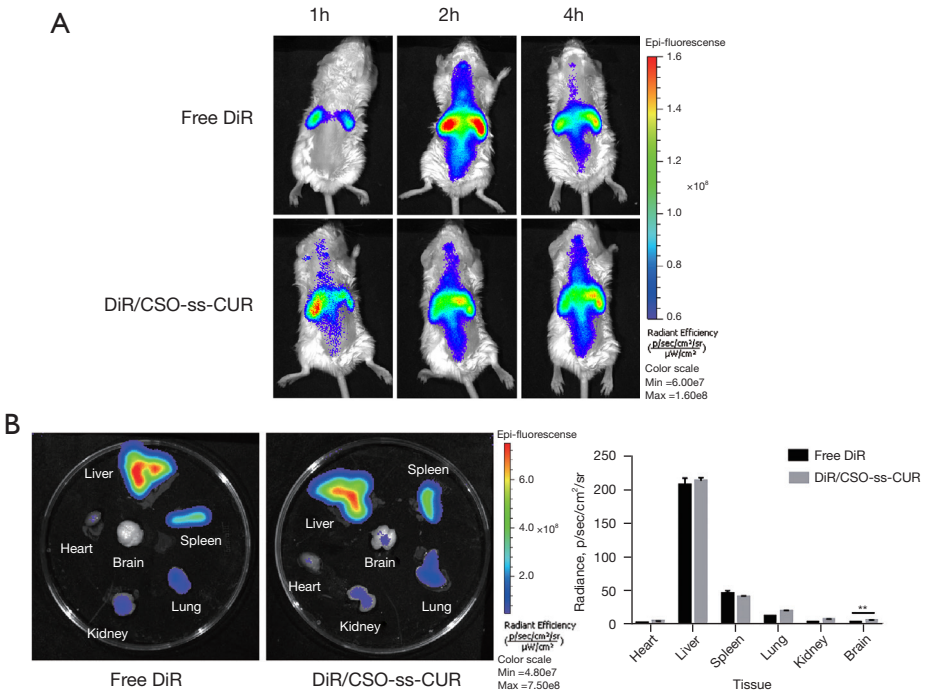

Figure 6 *In vivo* biodistribution of DTX-loaded nanoparticles. (A) Real-time fluorescence images of living mice following treatment with free DiR and DiR/CSO-ss-CUR through tail vein injection. (B) *In vitro* fluorescence imaging of the mouse organs after treatment with free DiR or DiR/CSO-ss-CUR through tail vein injection. **P<0.05. DiR, 1,1-dioctadecyl-3,3,3,3-tetramethylindotricarbocyanine iodide; CSO, chitosan oligosaccharide; CUR, curcumin; DTX, docetaxel.

551.02±118.00 mm^3 over 12 days (*Figure 5B,5C*). Moreover, mice treated with DTX/CSO-ss-CUR and DTX/CSO-cc-CUR exhibited significantly reduced tumor volume over the 12 days of treatment, from 115.00±14.52 to 75.67±51.79 mm^3 and from 115.88±15.17 to 225.77±123.19 mm^3, respectively (*Figure 5B,5C*). Compared with the NS group, mice treated with free DTX (Taxotere®) (P<0.01), DTX/CSO-ss-CUR (P<0.0001), and DTX/CSO-cc-CUR (P<0.0005) all showed apparent suppression of tumor growth. Moreover, mice treated with DTX/CSO-ss-CUR (P<0.001) and DTX/CSO-cc-CUR (P<0.005) exhibited significantly reduced tumor volume compared to mice administered free DTX (Taxotere®), indicating a better antitumor effect in both preparation groups. It is noteworthy that the DTX/CSO-ss-CUR group. Compared with DTX/CSO-cc-CUR group, the DTX/CSO-ss-CUR group showed excellent antitumor efficiency (P<0.05). Alterations in body weights were also monitored. There was no significant change in body weight in any of the treatment groups compared to the NS group. Mice in the free DTX (Taxotere®) group lost body weight slightly later during drug administration. In contrast, the weight of mice in the DTX/CSO-ss-CUR and DTX/CSO-cc-CUR groups increased slightly during the entire treatment regimen (*Figure 5D*), however, there was no statistically significant difference.

Histological analysis of the heart, liver, spleen, lungs, and kidneys showed that there were no significant histopathological changes and no significant damage to the primary tissues and organs in mice treated with DTX/CSO-ss-CUR, suggesting that this combined therapy is safe for *in vivo* applications (*Figure 5E*).

In vivo biodistribution of DTX-loaded nanoparticles

The real-time fluorescence images of free DiR and DiR/CSO-ss-CUR nanoparticles *in vivo* (*Figure 6A*) demonstrated that DiR/CSO-ss-CUR nanoparticles could be rapidly distributed in brain tissues and other tissues, and the fluorescence enhanced with the longer of time. while free DiR was present in a small amount in the brain only for a short time, the fluorescence intensity of free DiR increased before 2 h, and then decreased, suggesting that CSO-ss-CUR nanoparticles can penetrate the BBB rapidly

through blood circulation and deliver drugs to the targeted brain tissues, and maintain for a longer time than free DiR. This observation was consistent with previous findings that CSO, as a typical cationic polysaccharide, can bind tightly to the cell surface and mucosa, facilitating the opening of tight junctions, thereby increasing BBB penetration (21). Mice were sacrificed after 4 hours, and the main organs were dissected for fluorometric analysis. Interestingly, in mice treated with CSO-ss-CUR, strong DiR fluorescence was observed in the brain even *ex vivo* (*Figure 6B*).

Discussion

In all central nervous system diseases, malignant gliomas cause widespread concern due to high mortality and disability rates. Currently, surgical resection followed by concomitant radiotherapy or chemotherapy is applied for the treatment of malignant gliomas (6). However, the presence of BBB has severely hindered the progress of this strategy. BBB is one of the main physiological barriers of the human body and its low permeability severely hinders the penetration of drugs into the brain tissue for effective therapy (42). The main challenge in the treatment of glioma is to realize the accumulation of the effective drugs in the brain, to realize the targeted treatment of the glioma, and to limit the side effects of chemotherapeutic drugs. Although DTX is one of the most effective agents against gliomas (43), its therapeutic efficacy is often limited due to its severe adverse effects and poor BBB permeability. Thus, this current study developed brain targeting nanoparticles to enhance the chemotherapeutic sensitivity of DTX for gliomas. CUR was used as a part of the carrier material, acting as an antitumor drug and a DTX sensitizer. The therapeutic efficacy of these synthesized multifunctional nanoparticles was evaluated *in vitro* and *in vivo*.

CSO is an oligomer of chitosan with an average MW <10,000 Da. it display a significantly broad range of biological properties that confer a possible potential for drug delivery. Owing to its good water solubility, excellent biocompatibility, biodegradability, high chemical reactivity, easily functional and other significant biological properties (44), CSO has attracted great interest in pharmaceutics. it was also revealed that CSO can prolong the circulation time and have higher cellular transduction ability and could completely absorbed via intestinal epithelium depending on its cationic charge on their shorter N-glucosamine (N-Glc) units (45). CSO based nanocarriers can be used in ocular drug delivery depending on the good retention ability on the ocular surfaces, which could slow turnover rate of mucus layers. Recently, multiple lines of evidences have suggested that CSO possess good neuroprotective properties and increase the ability of the drugs to cross the BBB (21). In this paper, it was mainly verified whether CSO based drug delivery system could reach the brain to exert their antitumor effects. And the results of the study of the distribution of nanoparticles *in vivo* suggested that the nanoparticles formed by CSO-ss-CUR could successfully cross the BBB and delivered more drugs to the brain tissue to exert a therapeutic effect. And more importantly, the penetration ability of CSO-ss-CUR nanoparticles was mainly depended on CSO.

CAC is an important and commonly used parameter reflecting the self-assembled stability of nanoparticles. Usually, nanoparticles with a lower CAC can maintain their original morphology under extensive dilutions (36). In this study, the CAC was determined using a fluorescence probe of pyrene based on the ratio of its fluorescence intensity at 373 and 384 nm, and the changes of ratio with concentration can reflect the change of the microenvironment polarity of pyrene (46). The fluorescent spectrum of the pyrene probe will change once the pyrene encapsulated in the core of nanoparticles is released into the aqueous solution. The low CAC values of both CSO-ss-CUR and CSO-cc-CUR indicated that both of them can be self-assembled into nanoparticles at extremely low concentrations and have good stability in the blood circulation (47). In addition, the similar CAC values between CSO-ss-CUR and CSO-cc-CUR indicated that there was no significant difference between the self-assembly behavior of the conjugates with or without the disulfide bond, and this was consistent with the findings of previous study (48).

The mean particle size of each formulation showed a desirable diameter of 200 nm and a positive zeta potential. It has been shown that the size and zeta potential play a crucial role in the endocytosis of nanoparticles by brain endothelial cells (49). Generally, nanoparticles with a diameter around 200 nm and a positive zeta potential value are effective in crossing the BBB due to the enhanced permeability (50,51). The zeta potential values obtained for each composite were positive due to the polycationic amine groups from chitosan. It gives chitosan mucus adhesion ability to establish ionic interactions with anions on the cell surface or the mucosa, increasing resident time at the target site and enhancing membrane absorption (52). CSO is the only natural oligosaccharides with positive charges, which allows them to bind easily with other molecules via

hydrogen bonds and electrostatic forces (18).

The morphology of blank and DTX/CSO-ss-CUR nanoparticles under TEM revealed that the self-assembled nanoparticles had uniform spherical shape with uniform particle size, good dispersion, and no apparent aggregation. The particle size detected by TEM were consistent with those measured by DLS, although slightly smaller than the DLS results, mainly due to the differing methods of sample preparation, namely, the TEM samples are dry due to water loss while the DLS samples are aqueous solutions (37).

Due to uncontrollable cell growth and abnormal gene expression, the tumor microenvironment differs from other regular tissue sites and tends to be a substantial reductive environment (53). It was found that the redox-sensitivity properties could be used for the stable transportation of drugs in the body, to stimulate responses after reaching the tumor target tissue or target cells, and effectively control the delivery site and release speed of loaded drugs, thus significantly improving the target drug concentration, increase its antitumor activity, and reduce adverse reactions (54).

To evaluate the redox-sensitivity properties of the CSO-ss-CUR nanoparticles, the particle size was determined in the reductive environment at different concentrations of DTT. The CSO-ss-CUR nanoparticles containing the disulfide bonds may be easily degraded under reductive conditions. The size of the particles did not change during 24 hours without DTT, indicating that the nanoparticles were adequately stable. In contrast, the particle size of CSO-ss-CUR nanoparticles obviously changed under reductive conditions (10 mM DTT) and split from a single peak into multiple peaks within a few hours. These results confirmed that CSO-ss-CUR nanoparticles has redox-sensitivity properties, can respond to reductive intracellular conditions, and has the potential to effectively deliver drugs to the tumor site (55).

Redox-sensitivity was further confirmed by the *in vitro* release of DTX. In the first 12 hours, the cumulative release of DTX in PBS containing 10 mM DTT was more rapid (64.48%±9.75%) than in PBS without DTT (36.40%±1.70%). By 72 hours, the release reached approximately 87.93%±3.85% in the presence of DTT compared to 60.75%±9.34% in the absence DTT. The release of DTX/CSO-ss-CUR nanoparticles was significantly higher in release medium containing 10 mM DTT than in medium without DTT, confirming the redox-sensitivity of the nanoparticles and the potential to effectively release the drug in the tumor cells.

The hemolysis rate is an important indicator to certify the safety and blood stability of the constructed nanocarriers for intravenous injection. The hemolysis rate of the CSO-ss-CUR nanoparticles (at 0.1–1 mg/mL) was always less than 5%, satisfying the hemolysis requirements of intravenous preparations, indicating that these nanoparticles do not induce hemolysis in erythrocytes and have a good potential for *in vivo* application.

The *in vitro* cytotoxicity and live/dead cell assays demonstrated the superiority of combination therapy of DTX and CUR compared to the free drug. In addition, the higher cytotoxicity of the redox-sensitive DTX/CSO-ss-CUR nanoparticles compared to the non-redox-sensitive DTX/CSO-cc-CUR nanoparticles may be attributed to the more rapid drug release under the reductive conditions of tumor cells, which is consistent with the results of the *in vitro* release experiments. Compared with free C6, the intracellular fluorescence intensity of CSO-ss-CUR nanoparticles presented a positive correlation from 2 to 4 hours, indicating a time-dependent manner of cellular uptake. At 2 hours, part of the C6/CSO-ss-CUR nanoparticles were released faster and entered cells in the same manner as the free C6 group. Moreover, with the increase of time, the main cellular uptake mechanism of CSO-ss-CUR nanoparticles may be via the endocytosis pathway which is more efficient than free diffusion. Therefore, at 4 hours, the C6/CSO-ss-CUR nanoparticles showed much stronger fluorescence than that of free C6. The above results indicated that the CSO-ss-CUR nanoparticles could be absorbed by glioma cells in a short time and had good penetration to glioma cells.

In this study, the therapeutic efficiency and glioma inhibition ability of DTX/CSO-ss-CUR was investigated *in vivo*. Compared with the NS group, free DTX (Taxotere®), DTX/CSO-ss-CUR, and DTX/CSO-cc-CUR all showed apparent suppression of tumor growth in mice. Moreover, mice treated with DTX/CSO-ss-CUR or DTX/CSO-cc-CUR nanoparticles showed significant reduction in tumor volume compared to the free DTX (Taxotere®) group, indicating a better antitumor effect with both nanoparticles. This is mainly attributed to the longer circulation time of the nanoparticles *in vivo*, higher drug concentrations in the blood, tumor targeting, and DTX sensitization of CUR in the carriers. More importantly, after 12 days of treatment, only the DTX/CSO-ss-CUR group showed a remarkable reduction in tumor volume compared to day 0, confirming the antitumor potential of DTX/CSO-ss-CUR. Although the initial tumor volumes were

comparable with the DTX/CSO-cc-CUR group, higher glutathione (GSH) concentrations at the tumor site may allow the disulfide bonds in DTX/CSO-ss-CUR to quickly break and release the drug (56), reflecting the advantage of redox-sensitive nano-drug vector delivery systems. Furthermore, the H&E staining results of various tissues in tumor-bearing mice 12 days after administration showed no significant pathological change in the principal organs of the DTX/CSO-ss-CUR nanoparticle group compared to the NS group, indicating the excellent biocompatibility and safety of the delivery system (*Figure 5E*).

The change in body weight of tumor-bearing mice over the administration period was used as a vital evaluation indicator to reflect the toxicity and safety of each therapeutic agent. The body weight of mice in the free DTX (Taxotere®) group decreased slightly later in administration, consistent with the sluggish state of the mice later in administration, indicating some toxicity of free drugs. However, mice in the DTX/CSO-ss-CUR and DTX/CSO-cc-CUR nanoparticle groups, similar to the NS group, showed slight weight gain throughout the administration period, indicating that the preparation group was less toxic and the mice grew normally. Interestingly, mice in the NS group became thin while their body weights increased, and this may be due to growth in the tumor volume (57). The above *in vivo* antitumor studies confirmed that DTX/CSO-ss-CUR had optimum antitumor effects without significant systemic toxicity.

To study the distribution of nanoparticles *in vivo* and to verify whether the CSO-ss-CUR could pass through the BBB, DiR was used as a fluorescent marker and wrapped in CSO-ss-CUR nanoparticles using its hydrophobicity. The results showed higher fluorescence intensity in the brains of DiR/CSO-ss-CUR nanoparticles mice compared to mice treated with free DiR, suggesting that the nanoparticles formed by CSO-ss-CUR could successfully cross the BBB and deliver more drugs to the brain tissue to exert a therapeutic effect. While, the penetration ability of CSO-ss-CUR nanoparticles was mainly depended on CSO, which as a typical cationic polysaccharide, can bind tightly to the cell surface and mucosa, facilitating the opening of tight junctions, thereby increasing BBB penetration (21).

This is a preliminary pilot study exploring novel methods to improve the antitumor activity of DTX for malignant gliomas. Overall, the DTX/CSO-ss-CUR nanoparticles can be prepared via a stable method and exhibited superior brain tumor-targeting properties compared with free drugs. There were several limitations to this study. In particular, the mechanisms of therapeutic efficiency should be further investigated. Nonetheless, this report demonstrated that these newly developed nanoparticles have great potential for the treatment of brain-related diseases.

Conclusions

In summary, the redox-sensitive CSO-ss-CUR nanoparticles were designed as a carrier of the chemotherapeutic drug DTX. These nanoparticles enhanced the BBB permeability and improved tumor cell uptake, leading to more effective antitumor outcomes against gliomas. The accelerated release of the loaded drug from the DTX/CSO-ss-CUR nanoparticles was observed when exposed to a reductive release medium, demonstrating that the nanoparticles could rapidly release loaded drugs in the reductive environment. The DTX/CSO-ss-CUR nanoparticles were efficiently taken up by C6 glioma cells and enhanced anti-cancer activity when combined with free drugs. Moreover, the DTX/CSO-ss-CUR nanoparticles exhibited excellent brain targeting ability *in vivo* compared with free drugs. These results demonstrated that this novel nanoparticle may be a promising therapeutic strategy for the treatment of brain-related disorders.

Acknowledgments

Funding: None.

Footnote

Reporting Checklist: The authors have completed the ARRIVE reporting checklist. Available at https://atm.amegroups.com/article/view/10.21037/atm-22-288/rc

Data Sharing Statement: Available at https://atm.amegroups.com/article/view/10.21037/atm-22-288/dss

Conflicts of Interest: All authors have completed the ICMJE uniform disclosure form (available at https://atm.amegroups.com/article/view/10.21037/atm-22-288/coif). The authors have no conflicts of interest to declare.

Ethical Statement: The authors are accountable for all aspects of the work in ensuring that questions related to the accuracy or integrity of any part of the work are appropriately investigated and resolved. Experiments were performed under a project license [No. KYLL-2021(ZM)-011] granted by the Research Ethics Committee

of Qilu Hospital of Shandong University, in compliance with the Regulations of the People's Republic of China on the Management of Laboratory Animals (2017) for the care and use of animals.

References

1. McFaline-Figueroa JR, Lee EQ. Brain Tumors. Am J Med 2018;131:874-82.
2. Ostrom QT, Gittleman H, Truitt G, et al. CBTRUS Statistical Report: Primary Brain and Other Central Nervous System Tumors Diagnosed in the United States in 2011-2015. Neuro Oncol 2018;20:iv1-iv86.
3. Gao Y, Wang R, Zhao L, et al. Natural polymeric nanocarriers in malignant glioma drug delivery and targeting. J Drug Target 2021;29:960-73.
4. Louis DN, Perry A, Reifenberger G, et al. The 2016 World Health Organization Classification of Tumors of the Central Nervous System: a summary. Acta Neuropathol 2016;131:803-20.
5. Bleeker FE, Molenaar RJ, Leenstra S. Recent advances in the molecular understanding of glioblastoma. J Neurooncol 2012;108:11-27.
6. Gao H. Progress and perspectives on targeting nanoparticles for brain drug delivery. Acta Pharm Sin B 2016;6:268-86.
7. Zhao W, Yu X, Peng S, et al. Construction of nanomaterials as contrast agents or probes for glioma imaging. J Nanobiotechnology 2021;19:125.
8. Pang HH, Chen PY, Wei KC, et al. Convection-Enhanced Delivery of a Virus-Like Nanotherapeutic Agent with Dual-Modal Imaging for Besiegement and Eradication of Brain Tumors. Theranostics 2019;9:1752-63.
9. Mäger I, Meyer AH, Li J, et al. Targeting blood-brain-barrier transcytosis - perspectives for drug delivery. Neuropharmacology 2017;120:4-7.
10. Cui Q, Wang JQ, Assaraf YG, et al. Modulating ROS to overcome multidrug resistance in cancer. Drug Resist Updat 2018;41:1-25.
11. Hawasli AH, Kim AH, Dunn GP, et al. Stereotactic laser ablation of high-grade gliomas. Neurosurg Focus 2014;37:E1.
12. Chatterjee B, Gorain B, Mohananaidu K, et al. Targeted drug delivery to the brain via intranasal nanoemulsion: Available proof of concept and existing challenges. Int J Pharm 2019;565:258-68.
13. Barclay TG, Day CM, Petrovsky N, et al. Review of polysaccharide particle-based functional drug delivery. Carbohydr Polym 2019;221:94-112.
14. Sun Y, Jing X, Ma X, et al. Versatile Types of Polysaccharide-Based Drug Delivery Systems: From Strategic Design to Cancer Therapy. Int J Mol Sci 2020;21:9159.
15. Muanprasat C, Chatsudthipong V. Chitosan oligosaccharide: Biological activities and potential therapeutic applications. Pharmacol Ther 2017;170:80-97.
16. Liaqat F, Eltem R. Chitooligosaccharides and their biological activities: A comprehensive review. Carbohydr Polym 2018;184:243-59.
17. Yi Z, Luo X, Zhao L. Research Advances in Chitosan Oligosaccharides: From Multiple Biological Activities to Clinical Applications. Curr Med Chem 2020;27:5037-55.
18. Zhang J, Xia W, Liu P, et al. Chitosan modification and pharmaceutical/biomedical applications. Mar Drugs 2010;8:1962-87.
19. Jia L, Li Z, Zheng D, et al. A targeted and redox/pH-responsive chitosan oligosaccharide derivatives based nanohybrids for overcoming multidrug resistance of breast cancer cells. Carbohydr Polym 2021;251:117008.
20. Xu X, Sun L, Zhou L, et al. Functional chitosan oligosaccharide nanomicelles for topical ocular drug delivery of dexamethasone. Carbohydr Polym 2020;227:115356.
21. Zhu L, Li R, Jiao S, et al. Blood-Brain Barrier Permeable Chitosan Oligosaccharides Interfere with β-Amyloid Aggregation and Alleviate β-Amyloid Protein Mediated Neurotoxicity and Neuroinflammation in a Dose- and Degree of Polymerization-Dependent Manner. Mar Drugs 2020;18:488.
22. Zhao S, Pi C, Ye Y, et al. Recent advances of analogues of curcumin for treatment of cancer. Eur J Med Chem 2019;180:524-35.
23. Shafabakhsh R, Pourhanifeh MH, Mirzaei HR, et al. Targeting regulatory T cells by curcumin: A potential for cancer immunotherapy. Pharmacol Res 2019;147:104353.
24. Zangui M, Atkin SL, Majeed M, et al. Current evidence

and future perspectives for curcumin and its analogues as promising adjuncts to oxaliplatin: state-of-the-art. Pharmacol Res 2019;141:343-56.
25. Liu Z, Huang P, Law S, et al. Preventive Effect of Curcumin Against Chemotherapy-Induced Side-Effects. Front Pharmacol 2018;9:1374.
26. Li W, Zhang H, Assaraf YG, et al. Overcoming ABC transporter-mediated multidrug resistance: Molecular mechanisms and novel therapeutic drug strategies. Drug Resist Updat 2016;27:14-29.
27. Lopes-Rodrigues V, Sousa E, Vasconcelos MH. Curcumin as a Modulator of P-Glycoprotein in Cancer: Challenges and Perspectives. Pharmaceuticals (Basel) 2016.
28. Hou XL, Takahashi K, Tanaka K, et al. Curcuma drugs and curcumin regulate the expression and function of P-gp in Caco-2 cells in completely opposite ways. Int J Pharm 2008;358:224-9.
29. Choi BH, Kim CG, Lim Y, et al. Curcumin down-regulates the multidrug-resistance mdr1b gene by inhibiting the PI3K/Akt/NF kappa B pathway. Cancer Lett 2008;259:111-8.
30. Fratantonio D, Molonia MS, Bashllari R, et al. Curcumin potentiates the antitumor activity of Paclitaxel in rat glioma C6 cells. Phytomedicine 2019;55:23-30.
31. Gao H. Perspectives on Dual Targeting Delivery Systems for Brain Tumors. J Neuroimmune Pharmacol 2017;12:6-16.
32. Ju RJ, Mu LM, Li XT, et al. Development of functional docetaxel nanomicelles for treatment of brain glioma. Artif Cells Nanomed Biotechnol 2018;46:1180-90.
33. Sampath P, Rhines LD, DiMeco F, et al. Interstitial docetaxel (taxotere), carmustine and combined interstitial therapy: a novel treatment for experimental malignant glioma. J Neurooncol 2006;80:9-17.
34. O'Toole MG, Soucy PA, Chauhan R, et al. Release-Modulated Antioxidant Activity of a Composite Curcumin-Chitosan Polymer. Biomacromolecules 2016;17:1253-60.
35. Mu Y, Fu Y, Li J, et al. Multifunctional quercetin conjugated chitosan nano-micelles with P-gp inhibition and permeation enhancement of anticancer drug. Carbohydr Polym 2019;203:10-8.
36. Liu M, Du H, Zhai G. Self-assembled nanoparticles based on chondroitin sulfate-deoxycholic acid conjugates for docetaxel delivery: Effect of degree of substitution of deoxycholic acid. Colloids Surf B Biointerfaces 2016;146:235-44.
37. Mu Y, Wu G, Su C, et al. pH-sensitive amphiphilic chitosan-quercetin conjugate for intracellular delivery of doxorubicin enhancement. Carbohydr Polym 2019;223:115072.
38. Zhang D, Zhou W, Wei B, et al. Carboxyl-modified poly(vinyl alcohol)-crosslinked chitosan hydrogel films for potential wound dressing. Carbohydr Polym 2015;125:189-99.
39. Fan R, Chuan D, Hou H, et al. Development of a hybrid nanocarrier-recognizing tumor vasculature and penetrating the BBB for glioblastoma multi-targeting therapy. Nanoscale 2019;11:11285-304.
40. Hao Y, Zhang B, Zheng C, et al. The tumor-targeting core-shell structured DTX-loaded PLGA@Au nanoparticles for chemo-photothermal therapy and X-ray imaging. J Control Release 2015;220:545-55.
41. Gao H, Cao S, Yang Z, et al. Preparation,-Characterization and Anti-Glioma Effects of Docetaxel-Incorporated Albumin-Lipid Nanoparticles. J Biomed Nanotechnol 2015;11:2137-47.
42. Shi S, Fu W, Lin S, et al. Targeted and effective glioblastoma therapy via aptamer-modified tetrahedral framework nucleic acid-paclitaxel nanoconjugates that can pass the blood brain barrier. Nanomedicine 2019;21:102061.
43. Gaoe H, Pang Z, Pan S, et al. Anti-glioma effect and safety of docetaxel-loaded nanoemulsion. Arch Pharm Res 2012;35:333-41.
44. Wang Y, Khan A, Liu Y, et al. Chitosan oligosaccharide-based dual pH responsive nano-micelles for targeted delivery of hydrophobic drugs. Carbohydr Polym 2019;223:115061.
45. Naveed M, Phil L, Sohail M, et al. Chitosan oligosaccharide (COS): An overview. Int J Biol Macromol 2019;129:827-43.
46. Shi C, Zhang Z, Wang F, et al. Docetaxel-loaded PEO-PPO-PCL/TPGS mixed micelles for overcoming multidrug resistance and enhancing antitumor efficacy. J Mater Chem B 2015;3:4259-71.
47. Ou Y, Tang ZH, Sun L, et al. Combretastatin A4/poly(L-glutamic acid)-graft-PEG conjugates self-assembled to nanoparticles. Asian J Pharm Sci 2018;13:191-6.
48. Zhang J, Fang X, Li Z, et al. Redox-sensitive micelles composed of disulfide-linked Pluronic-linoleic acid for enhanced anticancer efficiency of brusatol. Int J Nanomedicine 2018;13:939-56.
49. Chauhan D, Sri S, Kumar R, et al. Evaluation of size, shape, and charge effect on the biological interaction and cellular uptake of cerium oxide nanostructures. Nanotechnology 2021. doi: 10.1088/1361-6528/ac03d5.

50. Caprifico AE, Foot PJS, Polycarpou E, et al. Overcoming the Blood-Brain Barrier: Functionalised Chitosan Nanocarriers. Pharmaceutics 2020;12:1013.
51. Alexis F, Pridgen E, Molnar LK, et al. Factors affecting the clearance and biodistribution of polymeric nanoparticles. Mol Pharm 2008;5:505-15.
52. Prabaharan M. Review paper: chitosan derivatives as promising materials for controlled drug delivery. J Biomater Appl 2008;23:5-36.
53. Xiao Y, Yu D. Tumor microenvironment as a therapeutic target in cancer. Pharmacol Ther 2021;221:107753.
54. Mollazadeh S, Mackiewicz M, Yazdimamaghani M. Recent advances in the redox-responsive drug delivery nanoplatforms: A chemical structure and physical property perspective. Mater Sci Eng C Mater Biol Appl 2021;118:111536.
55. Cai M, Wu Z, Li Y, et al. Bioinspired mimics: Self-assembly of redox-activated phosphorylcholine-based biodegradable copolymers for enhancing antitumor efficiency. Mater Sci Eng C Mater Biol Appl 2018;89:401-12.
56. Zhao S, Xu M, Cao C, et al. A redox-responsive strategy using mesoporous silica nanoparticles for co-delivery of siRNA and doxorubicin. J Mater Chem B 2017;5:6908-19.
57. Zhang X, Zhao L, Zhai G, et al. Multifunctional Polyethylene Glycol (PEG)-Poly (Lactic-Co-Glycolic Acid) (PLGA)-Based Nanoparticles Loading Doxorubicin and Tetrahydrocurcumin for Combined Chemoradiotherapy of Glioma. Med Sci Monit 2019;25:9737-51.

(English Language Editor: J. Teoh)

Cite this article as: Liu C, Gao Y, Zhao L, Wang R, Xie F, Zhai G, Liu A. The development of a redox-sensitive curcumin conjugated chitosan oligosaccharide nanocarrier for the efficient delivery of docetaxel to glioma cells. Ann Transl Med 2022;10(6):297. doi: 10.21037/atm-22-288

